

Design and Tuning of Wind Power Plant Voltage Controller with Embedded Application of Wind Turbines and STATCOMs

Lennart Petersen¹, Fitim Kryezi², Florin Iov³

¹Department of Energy Technology, Aalborg University, Aalborg 9220, Denmark (lep@et.aau.dk)

²Energinet.dk, Fredericia 7000, Denmark (fkr@energinet.dk)

³Department of Energy Technology, Aalborg University, Aalborg 9220, Denmark (fi@et.aau.dk)

Abstract: This paper addresses a detailed design and tuning of a wind power plant voltage control with reactive power contribution of wind turbines and STATCOMs. First, small-signal models of a single wind turbine and STATCOM are derived by using the state-space approach. A complete phasor model of the entire wind power plant is constructed, being appropriate for voltage control assessment. An exemplary wind power plant located in the United Kingdom and the corresponding grid code requirements are used as a base case. The final design and tuning process of the voltage controller results in a guidance, proposed for this particular control architecture. It provides qualitative outcomes regarding the parametrization of each individual control loop and how to adjust the voltage controller depending on different grid stiffnesses of the wind power plant connection. The performance of the voltage controller is analyzed by means of a real-time digital simulation system. The impact of discretizing the controller being initially developed in continuous-time domain is shown by various study cases.

Index terms: Wind Power, Voltage Control, Power Systems, State-Space Methods, Wind Power Plants, Renewable Energy

1. Introduction

Today's increasing amount of wind power penetration into the power system has engaged the wind power plants (WPPs) to take over the responsibility for adequate control of the node voltages, which has traditionally been accomplished by conventional power plants. This translates into more stringent requirements from the grid codes in different countries. Nowadays, voltage support at the point of common coupling (PCC) is achieved by an overall WPP controller, which distributes reference signals to the wind turbines (WTs), thus controlling the voltage at the PCC. However, due to the WTs' limited reactive power capability they may not fulfill the requirements for reactive power provision at the PCC. Moreover, long high-voltage alternating current (HVAC) cable connections in offshore WPPs (up to more than 150 km) will restrict the possibilities of WTs to contribute to plant voltage control. The integration of flexible alternating current transmission systems (FACTS) devices such as static synchronous compensators (STATCOM) is one way of dealing with this issue. Those fast-acting devices enhance in particular the dynamic performance, being a major concern in the presence of fluctuating wind power generation and involving challenges on small-disturbance voltage stability.

An overall plant voltage controller requires a high-performance and a robust solution in order to smoothly integrate all assets within the WPP. When dealing with control challenges in WPPs,

This article has been accepted for publication in a future issue of this journal, but has not been fully edited.

Content may change prior to final publication in an issue of the journal. To cite the paper please use the doi provided on the Digital Library page.

the majority of present research studies demonstrates their findings by time-domain simulations indicating the usage of numerical models. In [1] and [2] time-domain models of a whole WPP are developed and the performance of the plant controller is verified by numerical simulations. The studies offer quantitative measures regarding the control behaviour. However, they lack qualitative observations for the control development being particularly challenging for a large number of WTs and additional FACTS devices. Such analyses can be conducted in frequency domain by developing small-signal models for normal operational modes. In [3] the authors develop a complete small-signal model of the WT with direct-driven permanent magnet synchronous generator (PMSG) and assess the dynamic modes of the WT by Eigenvalue analysis. However, this study does not consider the model implementation of multiple WTs into an overall WPP. In [4] and [5] the small-signal approach is applied to model the entire WPP. However, the WPP is modelled as an aggregated model of one WT instead of a multi-turbine WPP representation, where the dynamics of the WTs are summarized to one aggregated time constant. Reducing the complexity of the WPP is advantageous considering the computation time required for control design. On the other hand, it can lead to reduced accuracy of the performed studies, as it lacks the actual dynamics occurring within the WPP. Moreover, the individual contribution of WTs and STATCOMs to voltage control cannot be investigated. The novelty of this paper resides in the modeling approach for voltage control analyses in wind power applications: a complex small-signal model of the whole WPP, introducing all individual units in order to enable the highest degree for the assessment of WPP voltage control (Section III). A WPP located in the United Kingdom (UK) and the corresponding grid code requirements are used as a benchmark case (Section II).

In terms of voltage control WPPs exhibit different characteristics than conventional generation plants. The main difference is the fluctuating power production requiring flexible and robust control for all operating points. Moreover, the large number of WTs introduces possible communication delays between plant controller and units being in a range of up to hundredths of milliseconds [5]. Furthermore, the control architecture is more complex, since the WPP controller needs to account for reactive power losses between WTs and PCC leading to additional control loops. As WPPs are erected in many different locations, often in rural wind-rich areas with weak network conditions, a large range of short-circuit ratios (SCRs) needs to be considered for the whole control design and tuning process. The dynamic requirements for controlling the voltage with a limited time delay, time response and overshoot are affected by all those aspects. They are examined in [5] for designing a slope voltage controller under various network configurations. However, in the literature there is no guidance available of how to parameterize the well-known controls for voltage control in WPPs, taking into account the dynamics of the individual assets, the expected time delays and various grid and operational conditions of the WPP. Thus, a step-by-step guideline to design and tune the WPP controller is required and is proposed by means of the elaborations made in section IV of this paper. The controller performance depending on the SCR as well as options for adjusted tuning to fulfill the grid code requirements are presented in section V.

For the sake of verifying the developed controllers, WPP models are commonly implemented in offline simulation tools such as DIGSILENT PowerFactory. However, in most cases the system including all controls is reproduced in continuous-time domain using the Laplace transform. When moving to practical implementation of the controls, nowadays digital control systems are employed which contain analog-to-digital converters (A/D) performing sampling of the sensor signals. Discrete-time equivalents need to be derived to approximate the behaviour of the original continuous-time controller, while all controller tasks need to be executed within one sample time period to prevent over-runs [6]. Hence, a deviating control performance is to be expected which

needs to be investigated prior to the system implementation in order for the WPP to become grid code compliant. In section VI of this paper the benchmark WPP system is analyzed by means of a real-time digital simulation platform in order to validate the voltage control performance.

2. System Description and Requirements

2.1. System Characterization of the Benchmark Wind Power Plant Network

For the purpose of this study a WPP located in the UK is used as benchmark. Therefore, the WPP takes into account general engineering rules for WPP topologies and the requirements for transmission systems in the UK. The WPP is comprised of 35 WTs of variable speed, full-scale power conversion and a power rating of 6 MW. The generated power of the WPP is transferred to the onshore grid through an export cable, where the PCC is defined at a rated voltage of 275 kV. Two STATCOMs with an respective MVA rating of ± 25 Mvar issue the WPP with additional reactive power provision closed to the PCC. The components of the benchmark WPP are summarized in Tab. 1.

Table 1 Components of benchmark offshore wind power plant

Plant Component	Voltage at Point of Connection
2 Supergrid Transformers	275/150/34 kV Onshore
2 STATCOMs	34 kV Onshore
Mechanically Switched Reactor	34 kV Onshore
Export Cable (29 km)	150 kV Onshore/Offshore
2 Offshore Transformers	150/34 kV Offshore
35 Wind Turbines	34 kV Offshore

2.2. Grid Code Requirements

The UK *Grid Code* [7] has the full responsibility of setting out the operating procedures and principles of power plants and also determines the relationship between the users of the *National Electricity Transmission System* (NETS) and the *National Grid Electricity Transmission* (NGET). The WPP voltage controller shall according to UK *Grid Codes* be able to perform a continuously automatic voltage control of the WPP without causing unintentional instabilities over its whole operation range. The corresponding grid code requirements regarding the reactive power response of the WPP are listed in Tab. 2. The important parameters are given by delay time (t_d), rise time (t_r), settling time (t_s) and the overshoot requirement (OS). Moreover, the control output signal shall not excite higher frequency oscillations in the network. The closed-loop system bandwidth shall be limited to 0 - 5 Hz being targeted for the control design in this study.

Table 2 Design requirements for voltage control

Parameter	Value	Unit
Delay time t_d	0.2	[s]
Rise time t_r	1.0	[s]
Settling time t_s	2.0	[s]
Overshoot	15	[%]

3.1. Wind Turbine Generators and STATCOMs

Nowadays WTs are equipped with full-scale converter systems being characterized by decoupling the two AC circuits on the machine and grid side respectively by the converter's DC-link. Due to this buffer between generator- and grid-side dynamics the WT system can be reduced to its grid-side converter (GSC), when the focus of analysis is laid on reactive power and voltage control. A reduced electrical model regarding only the GSC and its controllers in dq-reference frame is presented in Fig. 1.a). The mathematical description of the system is based on [3], though adapted for a GSC including reactive power control. The input power P_{SG} coming from the generator is simply represented by a constant DC current source feeding the DC-link (Eq. 1).

$$P_{SG} = I_{SG}V_{DC} \quad (1)$$

The expressions for the voltages v_{ACdq} at the AC terminal of the GSC are given by Eq. 2, where ω is the electrical angular velocity of the power grid voltage and L represents a series inductance of LC filter and step-up transformer assuming a high X/R ratio of those components [4, p. 51 ff.].

$$\begin{cases} v_{ACd} = L \frac{di_{ACd}}{dt} - \omega L i_{ACq} + v_{POCd} \\ v_{ACq} = L \frac{di_{ACq}}{dt} + \omega L i_{ACd} + v_{POCq} \end{cases} \quad (2)$$

The Phase-Lock Loop (PLL) will arrange the alignment of the dq-reference frame with the voltage at the point of connection (POC). Its dynamics imply a bandwidth of 100 Hz assuming a half-cycle from the fundamental grid frequency as the time constant of angle tracking process [9]. Hence, it is neglected for the reduced model of the WT, as it will not affect the dynamics of the overall WPP voltage controller. The active and reactive power output of the WT can be described by Eq. 3.

$$\begin{cases} P_{WTG} = \frac{3}{2} i_{ACd} v_{POCd} \\ Q_{WTG} = -\frac{3}{2} i_{ACq} v_{POCd} \end{cases} \quad (3)$$

The inner and outer control loops for the DC-link voltage and reactive power are depicted in Fig. 1.b). Four intermediate state variables φ_1 , φ_2 , φ_3 and φ_4 are introduced in order to express the dynamics of each PI controller (Eq. 4).

$$\begin{cases} \frac{d\varphi_1}{dt} = V_{DC} - V_{DC}^* \\ i_{ACd}^* = K_{P,DC}(V_{DC} - V_{DC}^*) + K_{I,DC}\varphi_1 \\ \frac{d\varphi_2}{dt} = i_{ACd}^* - i_{ACd} \\ v_{ACd}^* = K_{P,id}(i_{ACd}^* - i_{ACd}) + K_{I,id}\varphi_2 - \omega L i_{ACq} + v_{POCd} \\ \frac{d\varphi_3}{dt} = Q_{WTG} - Q_{WTG}^* \\ i_{ACq}^* = K_{P,Q}(Q_{WTG} - Q_{WTG}^*) + K_{I,Q}\varphi_3 \\ \frac{d\varphi_4}{dt} = i_{ACq}^* - i_{ACq} \\ v_{ACq}^* = K_{P,iq}(i_{ACq}^* - i_{ACq}) + K_{I,iq}\varphi_4 + \omega L i_{ACd} + v_{POCq} \end{cases} \quad (4)$$

Neglecting the high-frequency switching process so that $v_{ACd} = v_{ACd}^*$ and $v_{ACq} = v_{ACq}^*$, the dynamics of the current flowing across the inductance can be captured by Eq. 5.

$$\begin{cases} L \frac{di_{ACd}}{dt} = K_{P,id}(i_{ACd}^* - i_{ACd}) + K_{I,id}\varphi_2 \\ L \frac{di_{ACq}}{dt} = K_{P,iq}(i_{ACq}^* - i_{ACq}) + K_{I,iq}\varphi_4 \end{cases} \quad (5)$$

This article has been accepted for publication in a future issue of this journal, but has not been fully edited. Content may change prior to final publication in an issue of the journal. To cite the paper please use the doi provided on the Digital Library page.

The charging behaviour of the capacitor C determines the power balance of the DC-link (Eq. 6).

$$C \cdot V_{DC} \frac{dV_{DC}}{dt} = P_{SG} - P_{WTG} \quad (6)$$

Finally, the voltage angle δ_{POC} at the POC needs to be taken into account in order to link the individual dq-variables of the WT model to the phasor variables of the overall WPP model. The output currents are expressed using Forward Park Transformation (Eq. 7).

$$\begin{cases} i_{AC,Re} = i_{ACd} \cdot \cos \delta_{POC} - i_{ACq} \cdot \sin \delta_{POC} \\ i_{AC,Im} = i_{ACd} \cdot \sin \delta_{POC} + i_{ACq} \cdot \cos \delta_{POC} \end{cases} \quad (7)$$

Now the state-variables of the system are directly obtained by the dynamic equations (cp. Eq. 4 to 6), leading to state vector \mathbf{x} , while the remaining equations of this section make up the input vector \mathbf{u} and output vector \mathbf{y} of the state-space model.

$$\mathbf{x} = [\varphi_1 \ \varphi_2 \ \varphi_3 \ \varphi_4 \ i_{ACd} \ i_{ACq} \ V_{DC}]^T \quad (8)$$

$$\mathbf{u} = [Q_{WTG}^* \ V_{POC} \ \delta_{POC}]^T \quad (9)$$

$$\mathbf{y} = [i_{AC,Re} \ i_{AC,Im}]^T \quad (10)$$

By linearizing around steady-state values the linearized differential equations of the whole WT model are developed with resulting matrices \mathbf{A} , \mathbf{B} , \mathbf{C} and \mathbf{D} linking \mathbf{x} , \mathbf{u} and \mathbf{y} according to Eq. 11 [10] and can be found in [11].

$$\begin{aligned} \Delta \dot{\mathbf{x}} &= \mathbf{A} \Delta \mathbf{x} + \mathbf{B} \Delta \mathbf{u} \\ \Delta \mathbf{y} &= \mathbf{C} \Delta \mathbf{x} + \mathbf{D} \Delta \mathbf{u} \end{aligned} \quad (11)$$

By summarizing the Eigenvalues of the state matrix \mathbf{A} the relevant dynamics of the system are analyzed (Tab. 3). Eigenvalues λ_4 and λ_6 correspond to the dynamics of DC-link voltage controller and reactive power controller respectively. They exhibit frequencies around 2 Hz, hence being highly relevant for the overall voltage control of the WPP. The remaining Eigenvalues correspond to dynamics of the GSC exceeding the system bandwidth of 5 Hz and will not affect the relevant WPP control dynamics.

Table 3 System modes of WT state-space model

No.	Eigenvalue λ	Frequency [Hz]	Damping ratio	Time constant [s]	Dominant state
1	-9856	1568.68	1	0.0001	i_{ACd}
2	-801	127.53	1	0.0013	V_{DC}
3	-101	16.03	1	0.0099	φ_2
4	-14	2.16	1	0.0737	φ_1
5	-5872	934.57	1	0.0002	i_{ACq}
6	-13	2.12	1	0.0750	φ_3
7	-262	41.66	1	0.0038	φ_4

As the STATCOM exhibits the same topology of a grid-connected converter, just without active power production, the complete state-space model of the STATCOM is created according to the derivations and considerations for the WT model. A numerical EMT model is used to validate the state-space model of WT and STATCOM, showing that the linearized state-space model provides accurate results, even in the case of larger reactive power changes [11].

3.2. Wind Power Plant Network

For the components of the WPP network similar model considerations as for power flow studies are applied due to the low frequency area to be regarded for voltage control. Thus, transformers and external grid are modelled by an equivalent series RL impedance, while cables are expressed by the classical RLC π -model. Both C-type harmonic filters (HFs) and mechanically switched reactor (MSR) are represented by shunt admittances. [10]

All individual models are associated by linking the current injections, resulting from the state-space models of WT and STATCOM, and the bus voltages by the network impedances and admittances. However, it is insufficient for the state-space representation of the network to directly link currents and voltages by the impedance matrix of the networks. One has to notice that not only current injections influence the bus voltages, but also voltage changes of adjacent busses. In order to reflect this aspect, Eq. 12 originating from the power flow theory can be applied [12].

$$\bar{V}_i = \frac{1}{Y_{ii}} \left(\bar{I}_i - \sum_{j=1 \neq i}^n Y_{ij} \bar{V}_j \right) \quad i = 1 \dots n \quad (12)$$

The functional diagram of the WPP network model is depicted in Fig. 2.a). The respective voltage magnitudes and angles used as input variables for the WT model are achieved by Eq. 13, which needs to be linearized in order to yield a state-space representation of the overall WPP network model.

$$\begin{cases} V = \sqrt{V_{Re}^2 + V_{Im}^2} \\ \delta = \tan^{-1} \frac{V_{Im}}{V_{Re}} \end{cases} \quad (13)$$

The reactive power Q_{PCC} exchanged between WPP and external grid (Eq. 14) is used as control output signal for evaluating the voltage control performance.

$$Q_{PCC} = \frac{V_{PCC}(V_{PCC} - V_{grid} \cos \delta_{PCC})}{X_{grid}} \quad (14)$$

The resulting Multiple-Input-Multiple-Output (MIMO) system of the WPP with $\Delta \mathbf{Q}_{ref}$ as input signals and $\Delta \mathbf{V}$ is validated by means of load flow simulations in order to prove whether the change of network states are consistent with the actual power flow changes [11]. Fig. 2.b) represents one test case, where a reactive power change of $\Delta Q_{ref}^{WTG1 \dots 35} = 0.50$ pu for all WTs is applied to the state-space model, being linearized at $Q_0^{WTG1 \dots 35} = 0$ pu, and the resulting voltage deviation at all busses observed, while the voltage mismatch of two load flow simulations with $Q^{WTG1 \dots 35} = 0$ pu and $Q^{WTG1 \dots 35} = 0.50$ pu is used as basis of comparison. The maximum error of 0.76 % is within an acceptable range.

The complex state-space model is capable of representing the dynamic performance of the whole WPP with respect to small voltage disturbances, enabling to check reactive power capability limits by the individual WTs and STATCOMs as well as the voltage limits within the MV network. In this context, a further benefit is the capability of performing analyses for the WPP dispatch function, which has not been established yet in recent WPP control studies. Representing the overall system by phasor variables prevents the model from being subjected to any asymmetric disturbances. Small-signal linearization implies that for decent accuracy the model can only be used for the application of small-signal disturbances during normal operational mode. Large voltage excursions e.g. caused by short-circuits are according to grid codes typically to be handled at asset level, i.e. WT and STATCOM [13].

This article has been accepted for publication in a future issue of this journal, but has not been fully edited. Content may change prior to final publication in an issue of the journal. To cite the paper please use the doi provided on the Digital Library page.

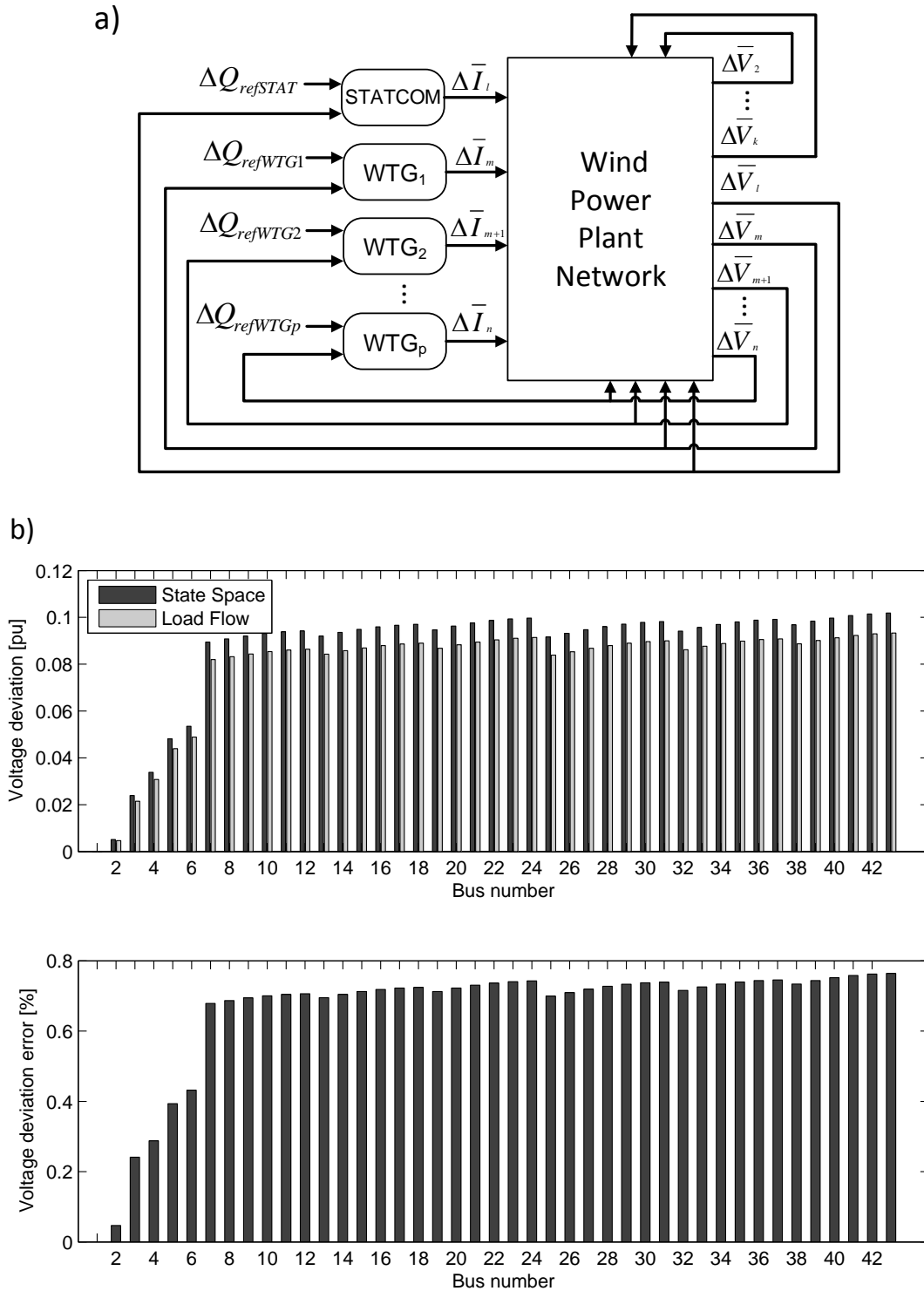


Figure 2. a) Functional diagram of wind power plant model used for the state-space representation, b) Voltage deviations of network busses with all WPP arrays connected to a strong grid, for a Q step change of $\Delta Q_{ref}^{WTG1...35} = 0.5$ pu.

This article has been accepted for publication in a future issue of this journal, but has not been fully edited. Content may change prior to final publication in an issue of the journal. To cite the paper please use the doi provided on the Digital Library page.

4. Design and Tuning of Wind Power Plant Controller

The WPP controller provides set-points to the individual WTs and STATCOMs and receives reference and measured feedback signals as shown in Fig. 3.a). The automatic voltage regulator (AVR)

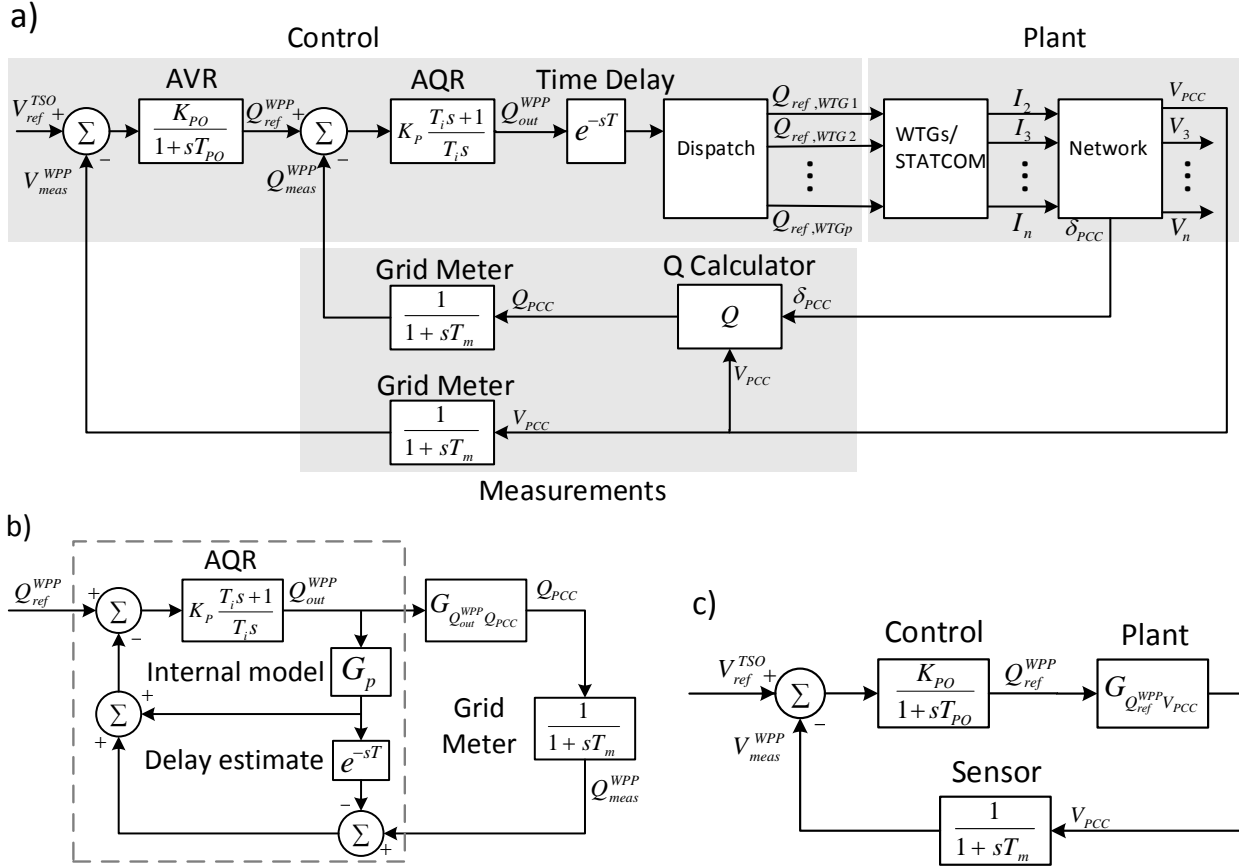


Figure 3. a) System representation for the overall wind power plant voltage control; b) Extended control structure of AQR with Smith Predictor; c) Control architecture used for AVR tuning

is characterized by slope control according to [7] with gain K_{PO} and time constant T_{PO} . The automatic reactive power regulator (AQR) accounts for the internal reactive power losses within the WPP in order to provide proper setpoints Q_{out}^{WPP} to the individual units. Several control strategies are possible for the AQR, e.g. by adding feed-forward signals to advance the response [13]. However, since commonly used in today's WPPs, the PI control approach serves as a benchmark strategy. In real-time control applications one need to regard the discrete sampling time as well as the computation time of the processor module and possible communication delays of signals being exchanged with the individual units in the WPP. The total system delay is modelled by e^{-sT} being linearized by first-order Pade function [13]. The signal distribution to the WTs and STATCOMs is illustrated by a dispatch block.

The design and tuning process for the WPP voltage controller should consider the whole operational range of a WPP and different grid conditions expressed by the short-circuit ratio (SCR) of the connected WPP. A stepwise design of AQR and AVR can be achieved by describing the whole WPP model by Single-Input-Single-Output (SISO) systems.

This article has been accepted for publication in a future issue of this journal, but has not been fully edited. Content may change prior to final publication in an issue of the journal. To cite the paper please use the doi provided on the Digital Library page.

4.1. Design of AQR

The practical application of Q ramp-rate limiters lowers the demand of fast response times for the PI controller of the inner loop AQR. In this case for its parametrization, the *Symmetrical Optimum* (SO) method is known to be an appropriate solution [14]. Therefore the high-order (60th) transfer function $G_{Q_{out}^{WPP}Q_{PCC}}(s)$, describing all the dynamics within the WPP and linking Q_{out}^{WPP} and Q_{PCC} (see Fig. 3.b), is reduced to a second-order system by MATLAB function *baldred(sys)*.

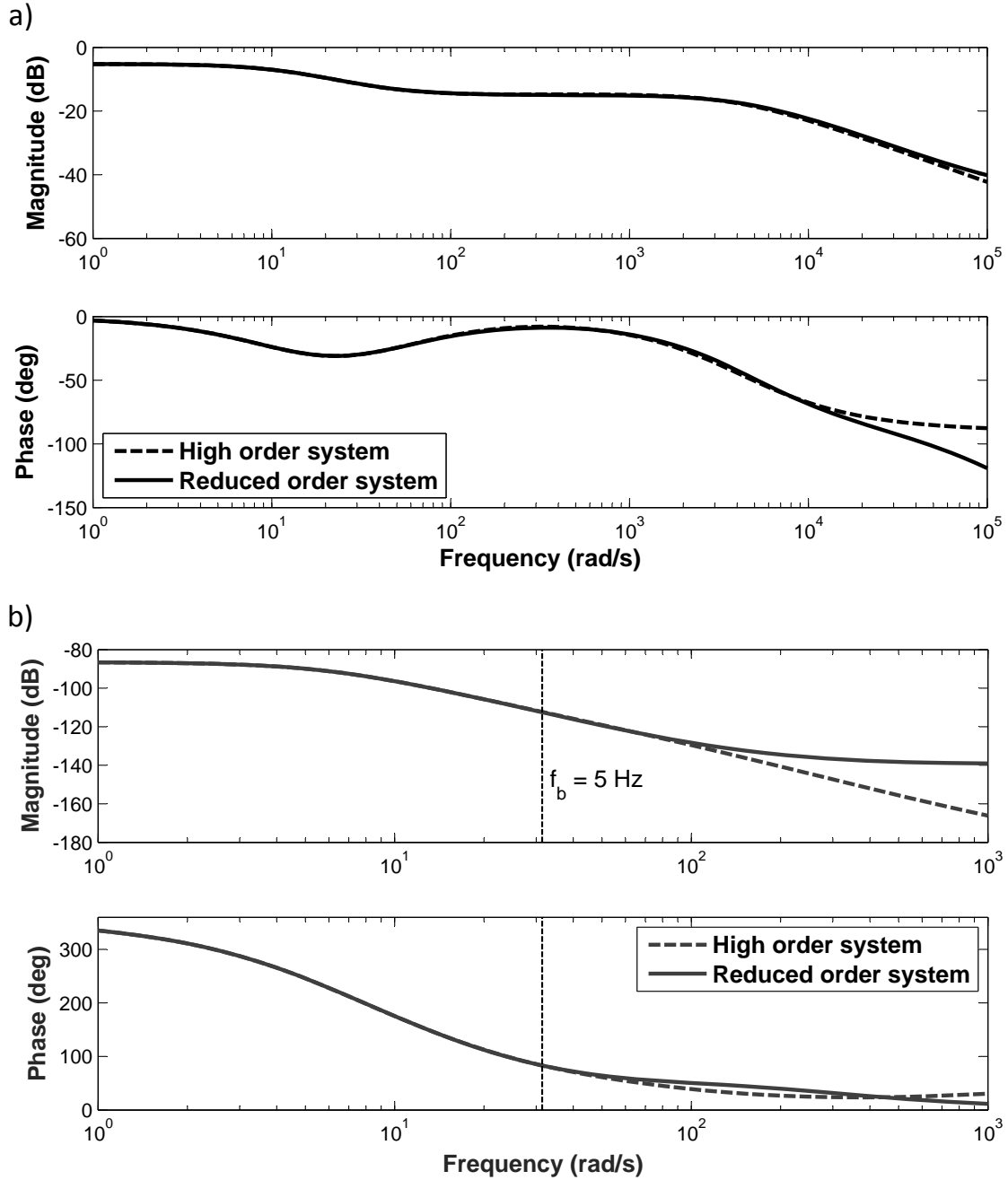


Figure 4. Frequency response of plant transfer functions for high-order system and reduced-order system: a) $G_{Q_{out}^{WPP}Q_{PCC}}(s)$ used for AQR design, b) $G_{Q_{ref}^{WPP}V_{PCC}}(s)$ used for AVR tuning

This article has been accepted for publication in a future issue of this journal, but has not been fully edited. Content may change prior to final publication in an issue of the journal. To cite the paper please use the doi provided on the Digital Library page.

As shown in Fig. 4.a) it exhibits an equal frequency characteristic in the relevant low frequency area (0 - 5 Hz). The PI control parameters T_i and K_p are obtained by second-order time constants T_1, T_2 and gain K_{plant} (Eq. 15) [11].

$$\begin{aligned} T_i &= 4k_1T_2 & k_1 &= \frac{1 + \left(\frac{T_2}{T_1}\right)^2}{\left(1 + \frac{T_2}{T_1}\right)^3} \\ K_p &= k_2 \frac{T_1}{2K_{plant}T_2} & k_1 &= \frac{1 + \left(\frac{T_2}{T_1}\right)^2}{\left(1 + \frac{T_2}{T_1}\right)^3} \end{aligned} \quad (15)$$

Since the plant transfer function $G_{Q_{out}^{WPP}Q_{PCC}}(s)$ is valid for one certain operational point of the WPP, the performance of the designed AQR is subject to variations. In particular, the operational state of the STATCOMs (on/off) affects the small-signal model of the whole WPP. Moreover, the possible time delays (e^{-sT}) need to be taken into account. This is realized by extending the system by a so called *Smith Predictor*, a type of predictive controller, which extends the plant transfer function $G_{Q_{out}^{WPP}Q_{PCC}}(s)$ by an internal model and a delay estimate as illustrated in Fig. 3.b). In [11] those aspects are elaborated more in detail.

4.2. Design and Tuning of AVR

The outer control loop AVR is designed and tuned according to the specifications of Tab. 2 to determine the dynamic performance of the system. Fig. 3.c) shows the default control architecture used for control analysis, which is realized in *Mathworks SISO Design Tool*. Again a high-order plant transfer function $G_{Q_{ref}^{WPP}V_{PCC}}(s)$ needs to be reduced by applying implicit balancing techniques [15]. Noticing that the WPP dynamics show a first-order behaviour and that one pole is introduced by the AQR as well as one more pole by possible time delays, the system is reduced to a third-order function. As illustrated by the bode plots in Fig. 4.b), it displays the same characteristics within the bandwidth of interest. Then the time constant T_{PO} of the slope controller should be selected according the bandwidth ω_b of the inner loop controller, namely the closed-loop system for AQR, by using Eq. 16 [13].

$$T_{PO} = \frac{1}{\omega_b} \quad (16)$$

The slope gain K_{PO} is determined by the TSO and can vary depending on the grid conditions and WPP location. The UK *Grid Code* stipulates a default slope setting of 4 % being applied in this study for an exemplary tuning process of the voltage controller. The resulting root locus plot of AVR open-loop system for a very stiff external grid with $SCR_{max} = 100$ is depicted in Fig. 5.a). The settling time requirement for t_s is related to the vertical line, while the allowed percent of overshoot (OS) is associated with the two rays, starting at the root locus origin. By observing the dashed encircled closed-loop poles, it can be seen for this exemplary case that the grid code requirements are fulfilled for this particular slope gain and grid conditions. However, since flexible slope changes are required depending on the WPP location, it is necessary to give full particulars to the voltage control performance as follows.

5. Performance Analysis of Voltage Control

Fig. 6 shows the results for a voltage step down of 5 % for a default slope of 4 % and two different grid stiffnesses SCR_{max} and SCR_{min} . For weaker grid conditions the performance of reactive

This article has been accepted for publication in a future issue of this journal, but has not been fully edited. Content may change prior to final publication in an issue of the journal. To cite the paper please use the doi provided on the Digital Library page.

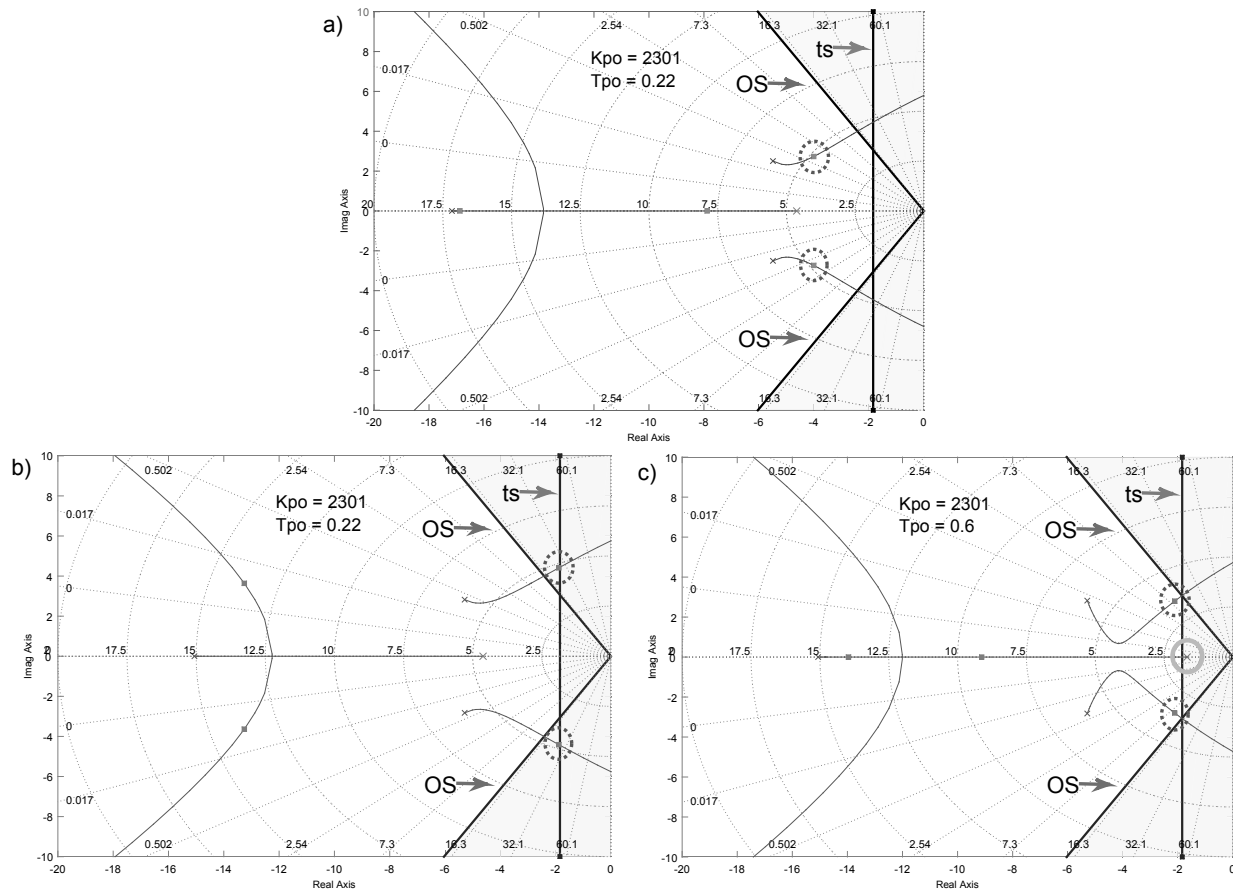


Figure 5. Root locus plot of AVR open-loop system with slope of 4 %: a) with SCR_{max} and $T_{PO} = 0.22$ s; b) with SCR_{min} and $T_{PO} = 0.22$ s; c) with SCR_{min} and $T_{PO} = 0.6$ s

power response is degraded with respect to overshoot and settling time. However, in [13] and [11] it is ascertained that the system performance is highly dependent on the open-loop gain of the system $K_T = X_{grid} \cdot K_{PO}$ which is composed of the external grid reactance and the slope gain. The proportional relationship of SCR and percentage slope is expressed by Eq. 17 and confirms why the voltage slope needs to be adjusted dependent on the grid conditions to obtain similar performance of the voltage controller [11].

$$SCR \cdot slope \sim K_T \quad (17)$$

Fig. 5.b) illustrates the obtained voltage control performance for SCR_{min} by root locus analysis. The design criteria are violated, as the system response will show too large overshoot. Now, a slope gain adjustment is possible, but depending on the connection agreements with the TSO the WPP operator is restricted by certain boundaries (in UK between 2 % and 7 %). A feasible alternative solution is to improve the voltage control performance by prolonging the time response of the AVR. Fig. 5.c) shows such a case: By moving to the right the solid encircled open-loop pole, being related to T_{PO} , the root locus plot is modified, so that the dashed encircled closed-loop poles are maintained inside the desired area. Based on the results presented in sections 4 and 5 a guidance for the design and tuning algorithm of a WPP voltage controller is presented in Fig. 7 and further elaborated in [11].

This article has been accepted for publication in a future issue of this journal, but has not been fully edited. Content may change prior to final publication in an issue of the journal. To cite the paper please use the doi provided on the Digital Library page.

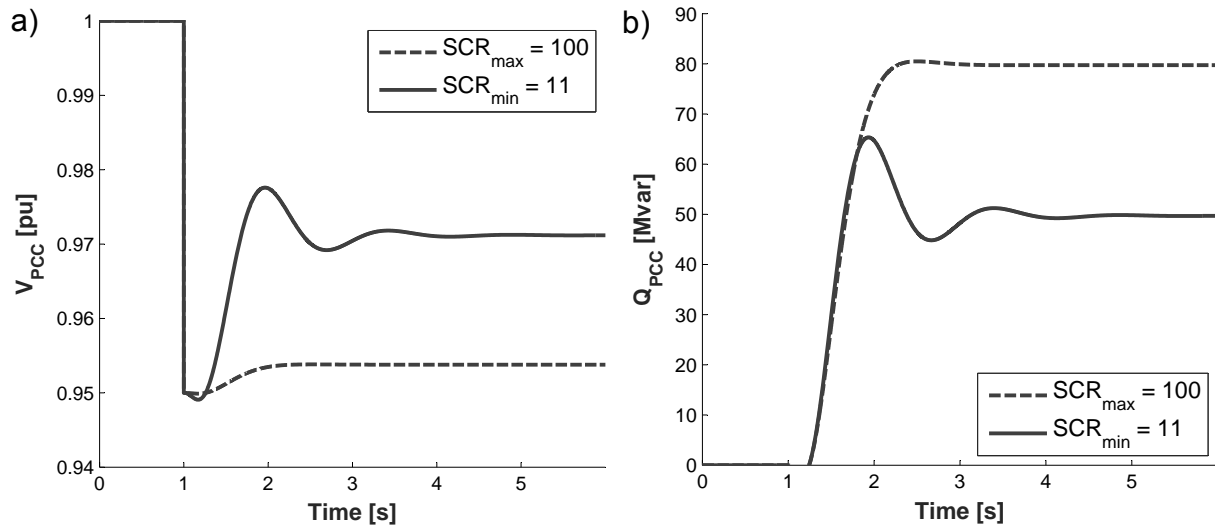


Figure 6. Voltage control performance for a slope of 4% and different grid stiffnesses SCR_{max} and SCR_{min} : a) PCC voltage; b) Reactive power at PCC

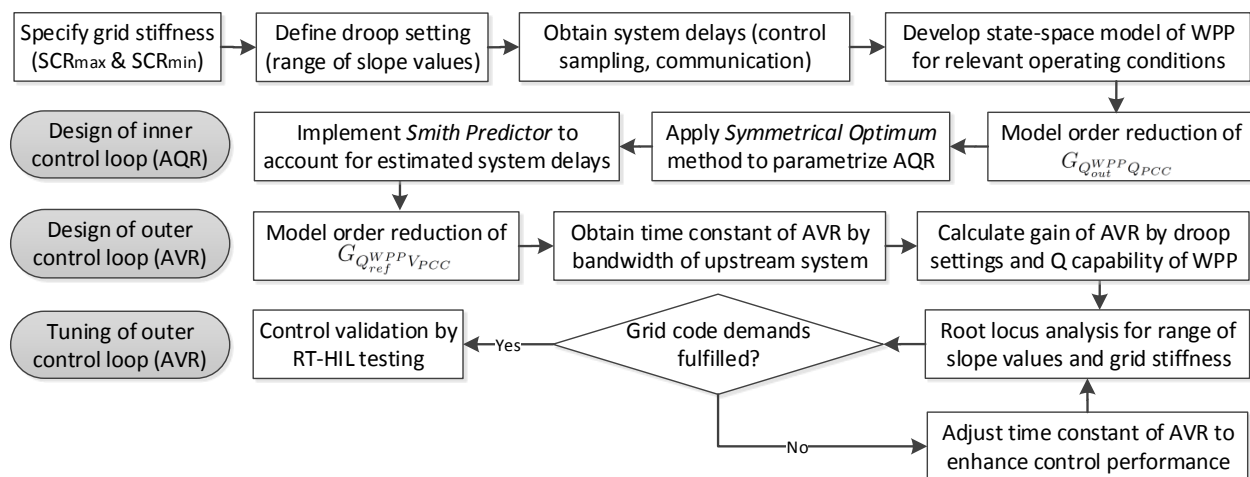


Figure 7. Guidance for design and tuning algorithm of wind power plant voltage controller

6. Verification and Validation by Real-Time Simulations

For the sake of verifying the design and tuning process, step responses for a voltage change are applied to the WPP system. The impact of different operating conditions, i.e. various initial active power values of the WTs, and the activation / deactivation of STATCOMs for additional reactive power contribution can be demonstrated by altering the state-space matrices of the system accordingly. Various relevant test cases are presented in [11].

However, in this publication the focus is laid on validation in a real-time simulation environment to study the performance of the voltage controller in a closed-loop discrete system. The whole WPP model is implemented in a real-time digital simulator based on *Opal-RT* technology in *Smart Energy Systems Laboratory* at Aalborg University [16]. The model is split into three parts each

This article has been accepted for publication in a future issue of this journal, but has not been fully edited. Content may change prior to final publication in an issue of the journal. To cite the paper please use the doi provided on the Digital Library page.

running on separate cores, where the assets (WTs and STATCOMs) are simulated with a sampling time of $T_{s,ass} = 1 \text{ ms}$ to account for the fastest dynamics captured, while the phasor-based WPP network runs with $T_{s,net} = 10 \text{ ms}$. As a base case, the WPP controller samples its reference signals with $T_{s,ctrl} = 100 \text{ ms}$, being a typical value for WPP control systems [17]. The subsequent test cases are performed for a relatively stiff grid characteristic ($SCR_{max} = 100$).

6.1. Controller Validation for Step Response

Fig. 8.a) shows an exemplary case where a step down in the PCC voltage is emulated by applying a disturbance of $\Delta V_{PCC} = V_{meas}^{WPP} - V_{ref}^{TSO} = -5\%$ to the voltage controller (see Fig. 3.a). The corresponding reactive power response is evaluated for the linearized state-space model running offline in s-domain and a closed-loop system running in real-time, where Backward Euler discretization method is chosen as a base case. The response requirements are indicated by the grey envelope. It can be observed that the real-time model takes a similar course compared to the offline case, thus fulfilling the grid code specifications according to the control tuning procedure. The immediate reactive power response to the step input is due to the feed-forward element of Backward Euler discretization. Additionally, it needs to be noted that an ideal communication between WPP controller and the units is assumed, neglecting possible signal delays.

6.2. Impact of Various Discretization Methods for Grid Voltage Disturbance

The previous test case reflects a typical example for on-site validation, where the performance of the WPP controller is tested by means of a simple step response. However, during normal operation the PCC is subject to continuous variations in the grid voltage involving the WPP controller to respond with reactive power provision. Fig. 8.b) depicts such a case with a sudden grid voltage step of $\Delta V_{grid} = -5\%$ considering two discretization methods. The reactive power response lags compared to the previous test case due to the reactive power drop in the very first instant caused by a sudden grid voltage drop (see Eq. 14).

The discrete-time equivalents can be derived by different approximation methods as for instance Backward Euler and Tustin approach. In Fig. 8.b) it can be observed that the discretization technique has significant influence on the performance, as Tustin method tends to overshoot in contrast to Backward Euler.

6.3. Impact of Various Control Sample Times

Another study case shall underline the impact of different control sample times on the performance of voltage control. The control sample time depend primarily on the employed communication technology, i.e. protocols and signal delays. As for instance, *Modbus/TCP* as commonly used communication protocol for the parameter exchange with STATCOMs processes the data query within 60 ms, without considering wire delays [18]. Hence, the control sample time needs to take on a larger value. Fig. 8.c) and 8.d) compare both considered discretization methods with halved and doubled values for the control sample time compared to the base case ($T_{s,ctrl} = 100 \text{ ms}$). The results imply that Backward Euler method offers a robust performance for various sample values. However, the second case (Tustin method) demonstrates that variations in $T_{s,ctrl}$ can lead to a defect control performance, considering the dynamic pattern of the reactive power output. Additionally, one needs to note that the value for sample time is limited due to aliasing effects. Noticing the obtained bandwidth frequency of the system $f_{b,max} = 1.34 \text{ Hz}$ [11], sample rates greater than the ones shown in Fig. 8.c) and 8.d) appear to be dangerously close to the Nyquist frequency.

This article has been accepted for publication in a future issue of this journal, but has not been fully edited. Content may change prior to final publication in an issue of the journal. To cite the paper please use the doi provided on the Digital Library page.

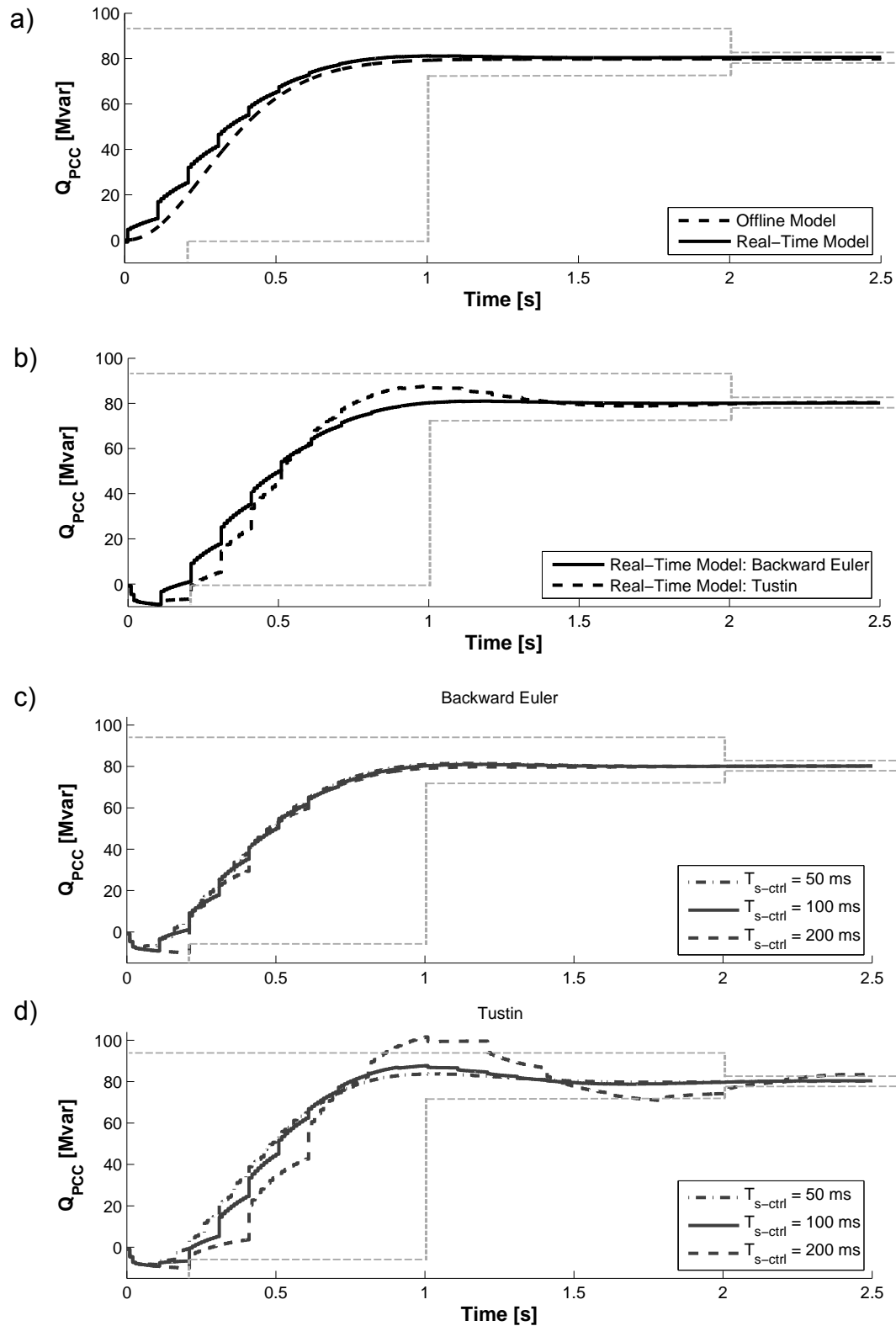


Figure 8. Reactive power responses: a) for step input to the state-space model and real-time model; b) for a grid voltage disturbance for different discretization methods; c & d) for a grid voltage disturbance for different control sample times

This article has been accepted for publication in a future issue of this journal, but has not been fully edited. Content may change prior to final publication in an issue of the journal. To cite the paper please use the doi provided on the Digital Library page.

6.4. Monitoring Internal Plant Behaviour

The real-time model enables to monitor all voltages within the WPP and the reactive power contributions of the individual assets as seen in Fig. 9. The voltages remain within the desired range of $\pm 10\%$ and in this study case the STATCOMs enhance the reactive power provision according to their dynamic capabilities, while the WTs remain within their capability limits of ± 3 Mvar.

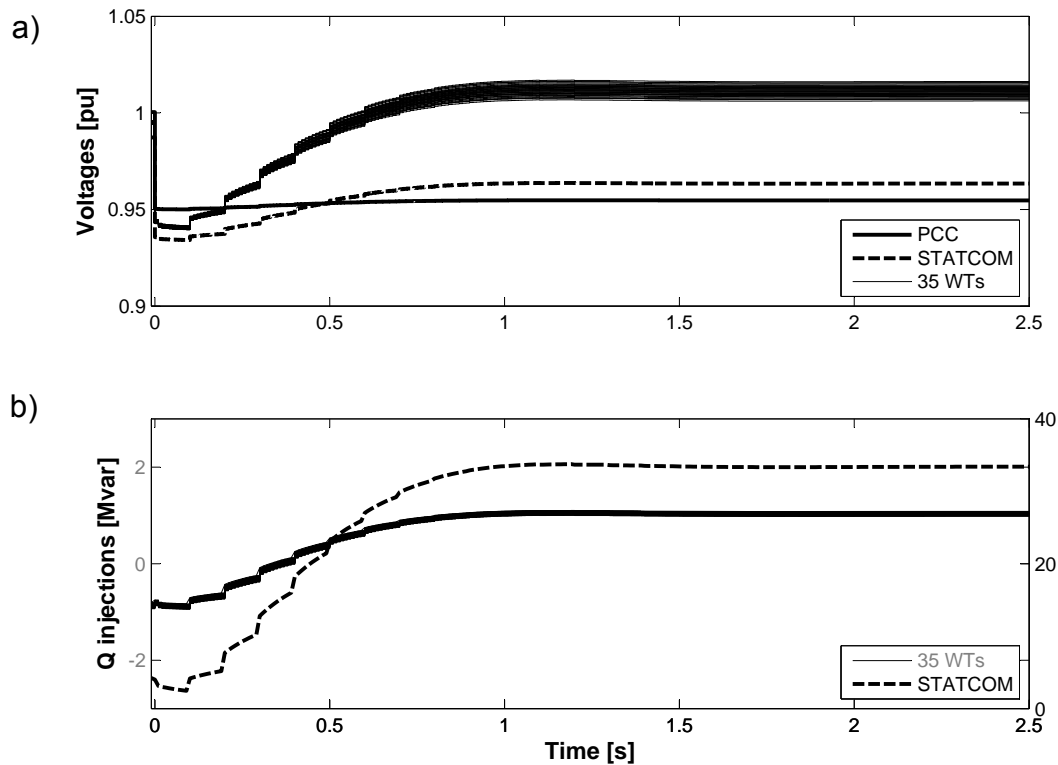


Figure 9. Feeder voltages (a) and reactive power injections (b) of wind turbines and STATCOMs for a grid voltage disturbance ($\Delta V_{grid} = -5\%$)

7. Conclusions

By developing a linearized model of the entire WPP system being suitable for voltage control analysis, this paper has introduced a step-by-step method for designing and tuning the WPP voltage controller and subsequently demonstrated its performance in a real-time simulation environment.

Initially, small-signal models of a WT and STATCOM are derived by using the state-space approach and the system dynamics being relevant for the overall voltage control are obtained by Eigenvalue analysis. A complete phasor model of the WPP is constructed by creating a MIMO state-space system, embedding all individual components of the WPP network and thereby enabling to analyze the full dynamic behaviour of the WPP as well as to investigate possible dispatch strategies for sending the reactive power signals to the individual WTs and STATCOMs. Connecting small-signal changes of voltages and currents are realized by considerations taken from the power flow theory, as it can be applied considering the small time constants involved in the network dynamics. The performance of the WPP network model is successfully validated against

load flow simulations.

The final development process of the WPP voltage controller delivers qualitative findings of how to treat the system transfer functions and their corresponding dynamics to design each individual control loop. Tuning the system according to grid code requirements is realized by root locus analysis, which eventually allows to analyze the benchmark WPP for different grid stiffnesses and to adjust the closed-loop poles accordingly.

The results validation by means of a real-time digital simulation system underlines the importance to analyze the control performance when moving from continuous-time to discrete-time domain. The reactive power response is successfully validated for the case of a step response applied to the system. However, the discretization method as well as the control sample time have a major impact on the control performance and need to be selected thoroughly taking into account the communication technology and signal delays present in the network.

Future work is intended for further testing the control performance under more sophisticated conditions being close to real system implementation by making use of the facilities in *Smart Energy Systems Laboratory* at Aalborg University [16]. It involves the integration of an industrial controller for hardware-in-the-loop testing as well as the network emulation with state-of-the-art communication protocols for wind power application to represent signal delays between controller hardware and simulated WPP units.

8. Acknowledgment

Parts of this paper have been presented at the 14th Wind Integration Workshop and published in the workshop's proceedings. Moreover, this paper is predominantly based on results of a MSc thesis, a project proposed by DONG Energy. The authors would like to thank Lukasz Hubert Kocewiak and Mikkel Peter Sidoroff Gryning from DONG Energy for all their support. The presented work is used in the PSO-forskell *RePlan* project "Ancillary Services from Renewable Power Plants" [19].

9. References

- [1] A. D. Hansen, P. Sørensen, F. Iov, and F. Blaabjerg, "Centralised power control of wind farm with doubly fed induction generators," *Renewable Energy*, vol. 31, no. 7, pp. 935–951, 2006.
- [2] J. Rodriguez-Amenedo, S. Arnaltes, and M. Rodriguez, "Operation and coordinated control of fixed and variable speed wind farms," *Renewable Energy*, vol. 33, no. 3, pp. 406–414, 2008.
- [3] H. Huang, C. Mao, J. Lu, and D. Wang, "Small-signal modelling and analysis of wind turbine with direct drive permanent magnet synchronous generator connected to power grid," *IET Renewable Power Generation*, vol. 6, no. 1, pp. 48–58, 2012.
- [4] A. G. Adamczyk, "Damping of low frequency power system oscillations with wind power plants," Ph.D. dissertation, Aalborg University, The Faculty of Engineering and Science, 2012.
- [5] J. Martinez, P. C. Kjær, P. Rodriguez, and R. Teodorescu, "Design and analysis of a slope voltage control for a dfig wind power plant," *IEEE Transactions on Energy Conversion*, vol. 27, no. 1, pp. 11–20, 2012.

- [6] M. S. Santina and A. R. Stubberud, "Discrete-time equivalents to continuous-time systems," *Control Systems, Robotics, and Automation - Vol.II*, 2009.
- [7] *National Grid Electricity Transmission The Grid Code. Issue 5. Revision 13 2015*, National Grid Electricity Transmission. Std.
- [8] J. Sun, "Small-signal methods for ac distributed power systems—a review," *Power Electronics, IEEE Transactions on*, vol. 24, no. 11, pp. 2545–2554, 2009.
- [9] B. Wen, D. Boroyevich, R. Burgos, P. Mattavelli, and Z. Shen, "Analysis of dq small-signal impedance of grid-tied inverters," *IEEE Transactions on Power Electronics*, vol. 31, pp. 675–687, 2015.
- [10] P. Kundur, N. J. Balu, and M. G. Lauby, *Power system stability and control*. McGraw-hill New York, 1994, vol. 7.
- [11] L. Petersen and F. Kryezi, *Wind Power Plant Control Optimisation with Embedded Application of Wind Turbines and STATCOMs*. Aalborg University, Department of Energy Technology, Aalborg ISBN: 978-87-92846-55-6, 2015.
- [12] IEEE, "Ieee recommended practice for industrial and commercial power systems analysis," 1997. [Online]. Available: <http://ieeexplore.ieee.org/stamp/stamp.jsp?tp=&arnumber=18478>
- [13] J. M. Garcia, *Voltage control in wind power plants with doubly fed generators*. Aalborg University, The Faculty of Engineering and Science, Department of Energy Technology, Aalborg, 2010.
- [14] E. Ceanga, C. Nichita, L. Protin, and N. A. Cutululis, "Theorie de la commande des systemes," *Ed. Tehnica, Bucarest*, 2001.
- [15] A. Varga, "Balancing free square-root algorithm for computing singular perturbation approximations," in *Proceedings of the 30th IEEE Conference on Decision and Control*. IEEE, 1991, pp. 1062–1065.
- [16] AAU, *Smart Energy Systems Laboratory, Aalborg University*. www.smart-energy-systems-lab.et.aau.dk, accessed June 2016.
- [17] K. N. Mehrdad Babazadeh, "Wind power plant control system, wind power plant including wind power plant control system and method of controlling wind power plant," *Patent: US20150219074 A1*, 2015.
- [18] M. Hewitt, "Technote 42 - modbus rs-485 timing issues," *Obvius*, 2012.
- [19] AAU, DTU, and Vestas, *RePlan Project "Ancillary Services from Renewable Power Plants"*. www.replanproject.dk, accessed June 2016.